"UNDERSTANDING THERMOELECTRIC PROPERTIES FROM DENSITY FUNCTIONAL THEORY"
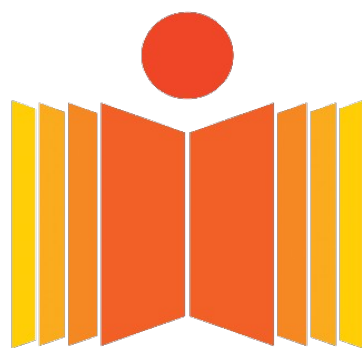
ASIM DAS

A Dissertation Submitted to

Indian Institute of Technology Hyderabad in partial

Fulfilment of the requirement for the degree of

Master of Science

भारतीय प्रौद्योगिकी संस्थान हैदराबाद
Indian Institute of Technology Hyderabad

Department of Physics

April, 2014

Declaration

I declare that this written submission represents my ideas in my own words, and where others' ideas or words have been included, I have adequately cited and referenced the original sources. I also declare that I have adhered to all principles of academic honesty and integrity and have not misrepresented or fabricated or falsified any idea/data/fact/source in my submission. I understand that any violation of the above will be a cause for disciplinary action by the Institute and can also evoke penal action from the sources that have thus not been properly cited, or from whom proper permission has not been taken when needed.
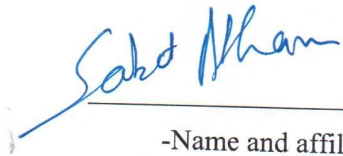
Asim Das

_____

(Signature)

_____ASIM DAS_____

(– Student Name –)
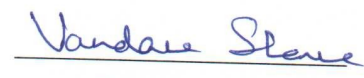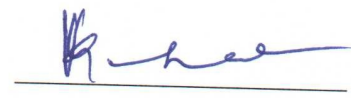
_____PH12M1003_____

(Roll No)

Approval Sheet

This thesis entitled "**UNDERSTANDING THERMOELECTRIC PROPERTIES FROM DENSITY FUNCTIONAL THEORY**" by ASIM DAS is approved for the degree of Master of Science from IIT Hyderabad.
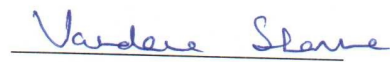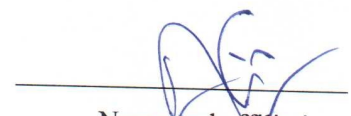
-Name and affiliation-

Examiner

-Name and affiliation-

Examiner

-Name and affiliation-

Adviser

-Name and affiliation-

Co-Adviser

-Name and affiliation-

Chairman

3

ACKNOWLEDGEMENTS

ABSTRACT

The electronic band structure and transport properties of SrAgFCh (Ch = S, Se, Te) are studiedusing the first principle density functional theory and solving the Boltzmann transport equationwithin the constant relaxation time approximation. The complete structural optimisation is carried out to get the ground state properties of all the compounds. The calculated ground stateproperties agree quite well with available experiments. The electronic band structures are calculated by means of the full-potential linear augmented plane wave method, using the Tran-Blahamodified Becke-Johnson potential and the calculated band gaps are found to be in good agreement with the experiments aswell as with other theoretical reports. The spin-orbit coupling shows a significant change in lifting the band degeneracy. Assuming constant relaxation time approximation, the transport coefficients related to thermoelectric effect are calculated by solving Boltzmann equation as implemented in BoltzTraP code. The calculated thermoelectric properties such as thermopower andelectrical conductivity as functions of hole and electron concentrations shows these compoundsto be promising candidate for better thermoelectric applications. The thermopower is found todecrease as we move from S to Te, whereas the electrical conductivity is found to be increaseand we also found that the investigated compounds are good candidate for p-type doping along the a-axis direction.

CONTENTS

Lists of figures

Lists of Tables

Chapter 1

Introduction

Thermoelectric materials convert waste heat into a useful electric power and hence play a vital role in meeting the present condition of energy crisis and environment pollution [1-4]. The performance of the thermoelectric materials depends on the dimensionless figure-of-merit **ZT**= $\frac{S^2 \sigma T}{\lambda}$ **,** where T, σ, S, λ are absolute temperature (T), electrical conductivity (σ), seeback coefficient (S) and thermal conductivity (λ) which include mainly two components: an electronic contribution due to the movement of carriers (λ_e), and a lattice contribution via the phonons λ_l) i.e ($\lambda = \lambda_e + \lambda_l$). From these expression, it is evident that finding materials with high ZT is a challenge, as it appears that such a material should satisfy the conflicting requirements of high thermopower, which is found in doped insulators and should behave as a good electrical conductor like metals with low thermal conductivity. In search for better thermoelectric materials, we are interested to study the newly synthesised quaternary strontium based silver fluoro-chalcogenides which belongs to the ZrCuSiAs-type structures. Compound with ZrCuSiAs type structure, often called as 1111 phases are increasing rapidly after it first discovery. More than 260 intermetallic compound with these structure are reported based on the possible combinations of the components and dopants [5-9]. These quaternary compounds, which belong to a much larger family of quaternary systems with the ZrCuSiAs typetetragonal structure (space group P4/nmm) possess broadly varying properties depending on their chemical composition—such as magnetic ordering, optical and opto-electronic characteristics and have diverse application in electronics [10], high temperature superconductors [11] thermoelectrics [12], optoelectronics [13], photovoltaics [14]. Presently, research have been focused to explore superconductivity and thermoelectric properties in ZrCuSiAs type structure.

In the past, oxygen-basedZrCuSiAs type of materials have been given much importance, which futher is extended to fluorides and hydrides [15]. Extensive studies have beenreported experimentally on these type of compounds, at the same time very less theoretical calculations are reported. The Fe-based 1111-phase compounds are reported to be the compounds with high superconducting transition temperature (T_c) so far [16-17]. The magnetic properties of the compounds includes dia-magnetism [15], itinerant ferromagnetic and semi-conducting anti-ferromagnetic nature [18-19]. The 1111-type of fluoro-pnictides has shown a wide range of thermopower of 10 to 620 $\frac{\mu V}{K}$ [20-22]. Recently synthesis of LaOAsS-type copper and silver based fluorides chalcogenides has given new insight to these class of materials [23]. On the other hand first principle calculations has reported the electric and optical properties on the same materials [24]. The presence flat band in the high symmetry k-direction of the electronic band structure has motivated us to study the thermoelectric properties of these class of materials as one could expect a good thermopower due to the flat-heavy bands at the fermi-level. The experimental band gaps are in the order of 2.23-3.0 eV, which can be classified as wide-band gap semiconductors, as semiconductors are the optimum materials to work for the better thermoelectric materials. Among these compounds we are interested to study the Sr-based silver fluorides chalcogenides i.e. SrFAgCh (Ch=S,Se,Te).

The present thesis is organized as follows: chapter 2 describes the theoretical background, and chapter 3 explains computational aspects of the present study. In chapter 4 we have presented the results and discussions, and finally chapter 5 gives the conclusions and future work.

Chapter 2

Theoretical Background

The fundamental postulates of quantum mechanics assert that microscopic system are described by wave function that completely characterize all the physical properties of the system called observables of various operators defined in quantum mechanics.

Considered a many body system having, P nucleons of charge Z_I at position R_I for n= 1,2,……… P and N electrons at position r_i for i=1,2,…N. The main interest is to find approximate solution of non-relativistic time independent Schrodinger equation.

HΨ=EΨ

Many body wave function is of form $\Psi = \Psi($ $R_1, R_2 \ldots. R_P ; r_1, r_2 \ldots \ldots r_N$) and E is the total energy of the system. The Hamiltonian H consists of following.

$$H \; \dot{\iota} \sum_{i=1}^{P} \frac{\hbar^2 \nabla_I^2}{2 M_I} - \sum_{i=1}^{N} \frac{\hbar^2 \nabla_i^2}{2 m_{\square}} + \frac{e^2}{2} \sum_{i=1}^{P} \sum_{j \neq i}^{P} \frac{Z_I Z_J}{R_I - R_J} + \frac{e^2}{2} \sum_{i=1}^{N} \sum_{j \neq i}^{N} \frac{1}{r_i - r_j} - e^2 \sum_{i=1}^{P} \sum_{i=1}^{N} \frac{Z_I}{R_I - r_i}$$

where R = { R_I }, I=1……..P, is a set of P nuclear coordinates, r= { r_i }, i=1……N, is a set of N electronic coordinates. $Z_I \wedge M_I$ are the nuclear charges and masses, respectively and e and m are electron charge and mass respectively. It includes kinetic energy (K.E) of all nucleus and electron, the inter nuclei repulsion energy, electron-electron repulsion energy and nuclei-electron attraction energy. In operator form we can write

$$H = T_n + T_e + V_{nn} + V_{en} + V_{ee}$$

Electrons are fermions, and the total electronic wave function must be anti-symmetric with respect to exchange of two electrons. Nuclei can be fermions, bosons or distinguishable particles according to the particular problem under consideration. All the ingredients are perfectly known and in principle, all the properties can be derived by solving the many body Schrodinger equation:

$$H \Psi_i (r,R) = E_i \Psi_i (r,R)$$

Although the equation is exact within the non-relativistic regime, it is not possible, except for trivially simple case to solve it. Consequently the many-body wave function is a complicated mathematical object that incorporates the effects of correlation, preventing the separation of the electronic degrees of freedom into single-body problems. Thus we must search for approximations that render the Schrodinger equation tractable to numerical solution, while retaining as much of the key physics as is possible.

2.1 **Approximation to solve Many-Body Problem**:

2.1.1 **Born-Oppenheimer Approximation:**

Since the electrons are much lighter than the nuclei by three orders of magnitude, makes nucleus almost immobile with reference to electrons. This can be exploited by treating the wave function in separable form, as

Ψ_i (r,R)=ϕ(r,R)χ(R)

where χ(R) is a nuclear wave function and ϕ(r,R) is an electronic wave function that depends parametrically on the nuclear positions. Besides this, we can neglect the term K.E of nuclei and consider the term nuclear-nuclear interaction as constant, so our Hamiltonian H reduces to

$$\text{H} ¿ \sum_{i=1}^{N} \frac{\hbar^2 \nabla_i^2}{2m_\square} + \frac{e^2}{2} \sum_{i=1}^{N} \sum_{j \neq 1}^{N} \frac{1}{r_i - r_j} - e^2 \sum_{I=1}^{P} \sum_{i=1}^{N} \frac{Z_I}{R_I - r_i}$$

2.1.2 Hartree-Fock Approximation:

Electrons are independent, and interact only via the mean-field coulomb potential.

Hartree took a different approach to consider the interacting electron via their own e-e electrostatic interaction and electron-nucleus electrostatic interaction. He thought that whole system can be assume as 'independent particle/electron' and interacting only through mean field coulomb potential. This lead to $\Phi_\square(r_1, r_2, r_3 \ldots \ldots r_N) = \Phi_1(r_1)\Phi_2(r_2)\Phi_3(r_3)$ …….. $\Phi_N(r_N)$

i.e. electron are independent. This yield one electron Schrodinger eq.

$$\{- \frac{\hbar^2 \nabla_r^2}{2m_e} + V_\square(r)\} \Phi_i(r) = \epsilon \Phi_i(r)$$

where V(r) is the potential in which electron move, this include both the nuclear and electron interaction.

$$V_{nucleus}(r) = -e^2 Z \sum \frac{1}{R}$$

And the mean field arises from the other N-1 electrons. We smear the other electrons out into a smooth negative charge density ρ(r') leading to a potential of the form

$$V_{electron}(r) = -e^2 \int \frac{\rho_j(r')}{Ir - r' I} dr$$

$$where \, \rho_i(r) \quad = \quad \sum_i | \phi_\square(r)|^2$$

Although these Hartree equations are numerically manipulable via the self-consistent field method, it is not surprising that such a crude approximation fails to capture elements of the essential physics. Since Pauli Exclusion Principle demands that the many-body wave function be anti-symmetric with respect to interchange of any two electron coordinates, e.g.

$$\Phi_\square(r_1, r_2, r_3 \ldots \ldots r_N) = -\Phi_\square(r_2, r_1 \ldots \ldots r_N)$$

This cannot be satisfied by a non-trivial wave function of the independent electron wave function form. This exchange condition can be satisfied by forming a slater determinant of single-particle orbitals

$$\Phi_\square(r_1, r_2, r_3 \ldots \ldots r_N) = \frac{1}{\sqrt{N}} A | \Phi_1(r_1) \Phi_2(r_2) \Phi_3(r_3) \quad \ldots \ldots \quad \Phi_N(r_N) |$$

where A is anti-symmetric operator, i.e. it ensure that all possible anti-symmetric combinations of orbitals are taken. Again, this decouples the electrons, leading to the single-particle Hartree-Fock equations of the form

$$\frac{\hbar^2 \nabla^2_\square}{2m_\square} \phi_i(r) + V_{electron}(r)\phi_i(r) + V_{nucleus}(r)\phi_i(r) \sum \int dr' \phi_j(r')_\square^{\,\dot\iota} \frac{1}{r_\square - r'} \phi_i(r')_\square^{\,\dot\iota} \phi_j(r) = \epsilon_i \phi_i(r)$$

The last term on the left hand side is the exchange term, this looks similar to the direct coulomb term, but for exchanged indices. It is a manifestation of the Pauli Exclusion Principle, and acts to separate electrons of the same spin. The exchange term adds considerably to the completely of these equations.

The Hartree-Fock equations deals with the exchange exactly, however, the equations neglect more detailed correlations due to many-body interactions. The effects of electronic correlations are not negligible; indeed the failure of Hartree-Fock theory to successfully incorporate correlation leads to one of its most celebrated failures. The requirement for a computationally practicable scheme that successfully incorporates the effects of both exchange and correlation and leads us to consider the conceptually simple and elegant Density Functional Theory.

2.2 Density Functional Theory:

Density Functional Theory (DFT), is a powerful formulation of many body quantum mechanics, which states that the ground state properties of a quantum many particle system depends only on density. In particular, the ground state density is found by minimizing the energy functional, whose value at minimum also gives the ground state energy. The electron density is defined as

$$\rho(r) = N \int \ldots \ldots \int |\Psi(r_1 r_2 \ldots r_N)|^2 dr_1 dr_2 \quad \ldots \ldots \quad dr_N$$

$\rho(r)$ determine the probability of finding any of the N electrons within the volume element dr_1 but with arbitrary spin, while other N-1 electrons spin and position in the state represented by Ψ. $\rho(r)$ is a non-negative function of only the three spatial variables which vanishes at infinity and integrate to total number of electrons

$$\rho(r \longrightarrow \infty) = 0 \text{ and } \int \rho(r) dr = N$$

2.3 Thomas Fermi Model:

The original density functional theory of quantum mechanics is the idea drawn from Thomas and Fermi proposed in 1927. Although their approximation is not accurate enough for present day electronic structure calculations, the approach illustrate the way to density functional theory. In the original Thomas-Fermi method, the K.E. of electrons is approximated as an explicit functional of density, idealised as non-interacting electrons in the homogenous gas with the density equal to the local density at any given point. Both Thomas and Fermi neglected the exchange and correlation among the electrons; however this was extended by Dirac in 1930, who formulated the local approximation for exchange still in use today. This lead to the energy functional for the electrons in an external potential $V_{ext}(r)$.

$$E_{TF}[n] = C_1 \int d^3 n(r)^{\frac{5}{3}} + \int d^3 r \, V_{ext}(r) \; n(r) + \; C_2 \int d^3 n(r)^{\frac{4}{3}} \; + \; \frac{1}{2} \int d^3 r \, d^3 \; r' \, n(r) \; \frac{1}{r_\square - r'} \; n(r')$$

Extension to account for the effect of inhomogeneity have been proposed by many people, known as the Weizsacker correction, $\dfrac{(\nabla n^\rho(r))^2}{4 n^\rho(r)}$ but more recent work has found the correction to reduce to

$\dfrac{(\nabla n^\rho(r))^2}{36 n^\rho(r)}$.

The attraction to DFT theory is evident by the fact that one equation for density is remarkably simpler than the full many body Schrodinger equation that involves 3N degree of freedom for N electrons. The Thomas Fermi approach starts with approximation that are too crude, missing the basic physics, such as shell structure and binding of molecules, thus it falls short of the goal of a useful description of electrons in matter.

2.4 Hohenberg-Kohn Equations:

Hohenberg, Kohn and Sham established a theoretical basis for justifying the replacement of the many body wave function by one-electron orbitals [25-27]. They used two fundamental theorems which leads to modern density functional theory, an alternative approach to deal with many body problem in electronic structural theory.

The charge density is a distribution of probability, i.e. $\rho(r_1) d^3 r_1$ represents, in a probabilistic way, the number of electrons in the infinitesimal volume ($d^3 r_1 ¿$. This applies to any system of interacting particles in an external potential $V_{ext}(r)$, including any problem of electrons and fixed nuclei, where the Hamiltonian can be written as H=T+V+U

$$T \equiv \frac{1}{2} \int \nabla \Psi^i(r) \nabla \Psi^\square(r) dr, \, V \equiv \int V(r) \Psi^i(r) \Psi^\square(r) dr, \; \text{U} \; \equiv \frac{1}{2} \int \Psi^i(r) \frac{1}{r_\square - r'} \Psi^i(r') \Psi(r') \Psi \, \overset{\overset{r}{¿ \, drdr'}}{¿}$$

Where T is K.E., U is interaction energy.

2.4.1 Hohenberg Theorems:

First theorems: "For any system of interacting particles in an external potential $V_{ext}(r)$, the total energy, is a unique functional of the electron density ρ(r)".

Second theorem: "A universal functional for the energy E[n] can be defined in terms of density. The density that minimizes the total energy is the exact ground state density".

2.5. Kohn-Sham equations:

Latter Kohn and Sham provided [25] a workable computational method based on the following result.

For each interacting electron system, there is a local potential V_{KS}, which result in a density ρ equal to that of interesting system. A lot of work was done to find T[n], V_{ee} [n] [Thomas, Fermi, Slater, Dirac etc], however the most successful approach come back to an 'exact expression' for the kinetic energy 'T', by re-introduce one body orbitals. To do that, Kohn-Sham introduced a fictitious equivalent system of non-interacting electrons under the action of an effective potential V_{eff} generating the same density ρ(r) of the real system.

$$\rho(r) \sum_{j=1....N} |\phi(r)|^2 \quad ...... (1)$$

and an orbital dependent exchange charge density ρ_i^{HF} for i^{th} orbital

$$\rho_i^{HF}(r,r') = \sum_{j=1...N} \frac{\phi_j^{\dot{c}}(r')\phi_i^{\dot{c}}(r')\phi_i^{\dot{c}}(r)\phi_i^{\square}(r)}{\phi_i^{\dot{c}}(r)\phi_i^{\square}(r)} \delta_{si,sj}$$

This density involves a 'spin' dependent factor which couples only (i,j) with the same spin coordinate (s_i , s_j). With these defined charge densities, it is possible to define corresponding potentials, the coulomb or Hartree potential ($V_H \dot{c}$, and is defined as

$$V_{HF}(r) = e^2 \int \frac{1}{r-r'} \rho(r)........... (2)$$

And an exchange potential can be defined as

$$V_X^i(r) = -e^2 \int d^3r' \frac{1}{r-r'} \rho_{HF}^i(r,r')$$

This combination results in the following Hartree-Fock equation

$$\{-\frac{\hbar^2\nabla_i^2}{2m_e} + V_N(r) + V_X^i(r)\}\Phi_i(r) = \epsilon\,\Phi_i(r)$$

Once the Hartree-Fock orbitals have been obtained, the total Hartree-Fock electronic energy of System, E_{HF} can be obtained from

$$E_{HF} = \sum_{i=1}^{N} E_i - \frac{1}{2}\int \rho(r)V_H d^3r - \frac{1}{2}\sum E_i \int \Phi_i^{\dot{c}}(r)\Phi_i(r)V_i^X(r)d^3r$$

Thus the Kohn-Sham energy functional is formally written as

$$H_{KS} = \frac{\hbar^2\nabla_\square^2}{2m_\square} + V_{eff}............(3)$$

Where the effective potential is define as for an one-electron potential, i.e.

$$V_{eff} = V_N(\rho) + V_H(\rho) + V_{XC}(\rho)$$

E_{HF} is not a sum of the Hartree-Fock orbitals energy E_i. The factor of one half in the e-e terms arises since the e-e interactions have been double counted in the coulomb and exchange potentials. The Hartree-Fock Schrodinger equation is slightly more complex than the Hartree equation.

Note that in contrast with equation

$$H_{KS} = \Sigma \frac{-\hbar^2 \nabla_i^2}{2m_\square} + V_N$$

V_{XC} is now without an index, as it is only for one electron. Also note the dependence of each potential term on the charge density $\rho_{\text{¿}}$), which is implicitly defined from the set of occupied energies Ψ_i, i=1…N of the equation (3) eqby (1). The energy term associated with the nuclei-electron interaction is $¿V_N I \rho > ¿$, while that of e-e interaction is $¿V_H I \rho > ¿$, where V_H is Hartree potential.

$$V_H(r) = \int \frac{1}{r-r'} \rho(r') dr'$$

The Kohn-Sham energy Functional is of the following form

$$E(\rho) = \frac{\hbar^2}{2m_\square} \sum \int \phi_i^r \nabla_\square^2 \phi_i \, dr + \int \rho(r) V_{ion}(r) dr + \frac{1}{2} \int \frac{1}{r-r'} \rho(r') dr dr' \quad + \quad E_{XC}(\rho(r))$$

And the Kohn-Sham equation for electronic structure of matter is given as

$$\{ -\frac{\hbar^2 \nabla_i^2}{2m_e} + V_N(r) + V_H(r) + V_{XC}(\rho(r)) \} \Phi_i(r) = E_i \Phi_i(r)$$

This equation is usually solved 'self-consistently'. An approximate charge is assumed to estimate the exchange-correlation potential, and this charge is used to determine the Hartree potential from eq-(2). These approximate potentials are inserted in Kohn-Sham equation and the total charge density is determined as in eq-(1). The output charge density is used to construct new exchange correlation and Hartree potentials. The process is repeated until the input and output charge density or potentials are identical within some tolerable limit. Once self-consistency is achieved, a solution of the kohn-Sham equation is obtained, and the total energy can be written as

$$E_{KS} = \sum_{i=1}^{N} E_i - \frac{1}{2} \int \rho(r) V_H d^3 r - \int \rho(r) E_{XC}(\rho(r)) - V_{XC}(\rho(r)) d^3 r$$

The algorithm of this self-consistent algorithm is shown in fig-2.1

2.5.1 Local Density Approximation (LDA)

LDA approximation is a key contribution by Kohn-Sham, which for computations of the quantum ground state of many-particle systems proved to be superior to both Thomas-Fermi and Hartree-Fock theories, the basis of the local density approximation for the exchange and correlation energy functional is the theory of the homogeneous electron liquid. This is a most important model system, which of course does not exist in nature, but which can nowadays theoretically be treated with extremely high precision. So that E_{xc} depends only on the local electron density around each volume element dr in the system.

Exchange Correlation Functional can be represented as

$$E_{xc}[n] = \int n(r)\varepsilon_{xc}[n(r)]dr$$

where $\varepsilon_{xc}[n(r)]$ is the energy density in homogeneous electron gas.

It provides us with much successful results than expected, especially for solid, who's structural and vibrational properties are in general well described. LDA yields results that compare well to HF results even for molecules and atoms. LDA is computationally much simpler than HF with the true exchange potential. It gives the correct crystal structure which is usually found to have the lowest energy, bond lengths, bulk moduli, phonon frequencies which are accurate within a few percent.

LDA provides a good description of the spherical term of the so-called "exchange-correlation hole".

2.5.2 Generalised Gradient Approximation (GGA)

As the LDA approximate the energy of the true density by the energy of a local constant density, it fails in the situations where the density undergoes rapid change such as in molecules. An improvement to this situation can be made by considering the gradient of the electron density, so called Generalised Gradient Approximation, symbolically it can be written as

$$E_{GGA}^{XC} = \int f[n(\mathbf{r}), \nabla_{\mathbf{r}} n(\mathbf{r})]d\mathbf{r}$$

This can lead to large improvement over LDA result.

Some of these are semi-empirical, in that experimental data e.g atomization energy is useful in their derivation. A commonly used functional are PBE, PW91 functional, due to Predew-Burke-Ernzerhof parameterization, Perdew and Yan respectively.

Algorithm of Self-Consistent Calculation

Initial guess for

SETTING UP THE

SOLVING KOHN-
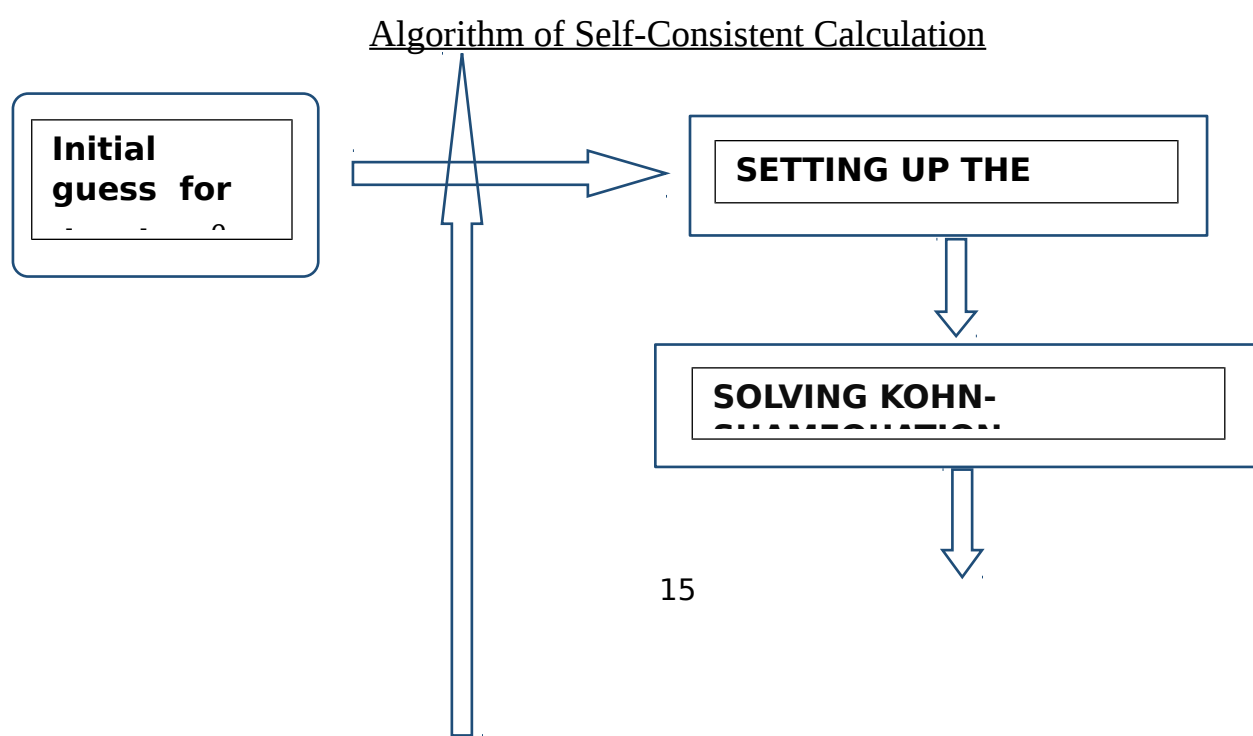
Fig-2.1: Algorithm for self-consistent

2.6. Introduction to Thermoelectric Materials

The quest for better, cost effective, high temperature thermoelectric materials has resulted in intensive research, due to the development of new materials and fabrication technologies, since it is an ideal solution for sustainable energy, to meet the current energy demand. Though the efficiency of thermoelectric materials are low they are now seen as new green e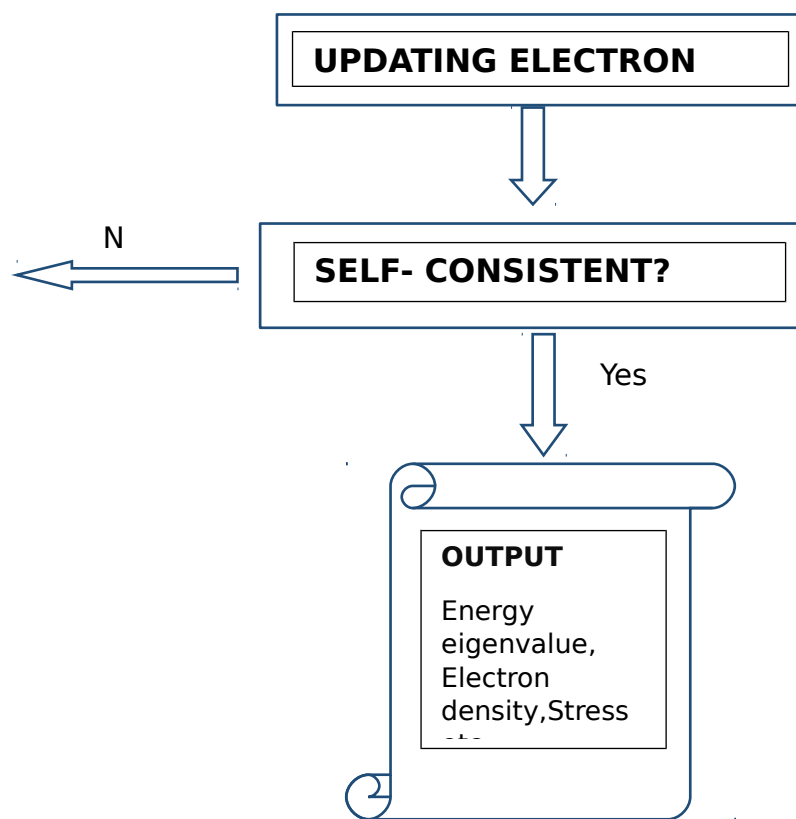nergy source because of its ability to generate electricity from waste heat. Therefore, looking at possibilities to improve the thermoelectric efficiency becomes the key issue in the research field [28].

In solids electrons not only conduct electricity but also conduct heat. These two phenomenon are coupled, since electrical conductivity transport energy and thermal conductivity transport charge from hot junction to cold junction. Thus this coupling between electrical and thermal transport give rise to thermoelectric phenomenon [29-31]. Thermoelectric materials show thermoelectric effect i.e either a temperature difference can create an electric potential or a potential difference can create a temperature difference and their major application lies in (micro) cooling or electricity generation from heat sources. There are three types of thermoelectric effect.

1. Seebeck Effect

If two wires of dissimilar metal joined end to end and two junctions are maintained at different temperature i.e connected electrically in series and thermally in parallel, then a current flows through the circuit. This is known as Seebeck Effect. Such a current is known as thermoelectric current and emf producing it is called thermo-emf, was first reported by Thomas Seebeck in 1821. The circuit formed by the two wires of dissimilar metals is called thermocouple. The direction and magnitude of the Seebeck voltage (V), depends on the temperature difference between the two junctions of the thermocouple and on the materials making up the thermocouple i.e on the Seebeck coefficient (S) [32].

$\Delta V = S \Delta T$, where S is Seebeck coefficient (also known as thermo power, thermoelectric power, thermoelectric sensitivity) of the material, measure the magnitude of the thermoelectric voltage (ΔV) in response to the temperature difference (ΔT) across the material. It is also defined as the entropy transported with a charge carrier divided by the carrier's charge [33]. The materials A and B of the thermocouple must be p-type or n-type, for an exchange between electrons and holes or vice versa at the junctions T_1 and T_2 (see Fig-2.1), completing the circuit and allowing for either power generation or refrigeration.The sign of the Seebeck coefficient is determined by the direction of current flow. If T_2 is greater than T_1 and the current is flowing clockwise than the Seebeck coefficient is positive meaning the material is n-type, and if the current is counter-clockwise it is negative [34] meaning the material is p-type.
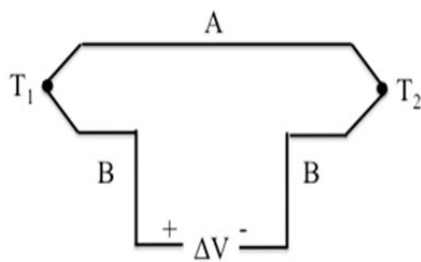

Fig-2.2: Measuring the Seebeck Effect of two dissimilar
metal A, B when kept at different temperature   (wikipedia image)

2. Peltier Effect

If a current is made to flow through the circuit of two dissimilar metals by using an external source then one junction gets heated whereas other gets cooled, depending on the direction of current flow, this phenomenon is known as Peltier Effect [29], the heat evolved or absorbed as Peltier heat. The rate of heating or cooling at a junction is found to be proportional to the strength of the current and changes it's sign on reversing the direction of current. Thus Peltier effect is reversible. The effect is just the reverse of the Seebeck Effect. Thus materials exhibiting a large Seebeck effect also show a large Peltier effect. The effect can be quantitatively described by the Peltier coefficient ($\pi \dot{\iota}$, (see Fig-2.3). The Peltier coefficient (π) is determined by the ratio of the rate of heating (Q) to the current (I) i.e ($\pi = \dfrac{Q}{I}$). The Peltier heat generated at the junction per unit time, Q is equal to $Q = \dot{\iota}^{\pi_a - \pi_b}$) I, where, π_A and π_B is the Peltier coefficient of conductor A and B, and measure the amount of heat evolved or absorbed, when unit current pass through the thermocouple junction, and I is the electric current (from A to B). The sign of π is determined by junction getting heated or is cooled. In Fig-2, if T_1 is cooled and T_2 is heated,

then the Peltier coefficient is positive, and negative in the reverse situation when the current flows the opposite direction.
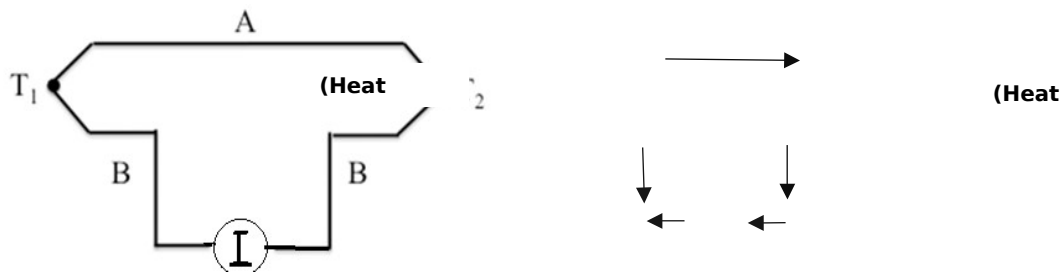

Fig-2.3: Measuring the Peltier Effect of two dissimilar metal A, B when current flow through the junction in clockwise direction, causing heating or cooling of one junction (wikipedia image)

3. Thomson Effect

In order to connect the thermoelectric effects as observed by Seebeck and Peltier, William Thomson described the third thermoelectric effect, Thomson effect which describes the resulting electric current that develops in a single conductor when a small temperature gradient is applied [29-31]. This relationship is described by the equationQ=βIΔT, where Q is the rate of heating, I is electric current, ΔT is change in temperature, and β is the Thomson coefficient. This relationship holds if the temperature difference, ΔT, is small.

Lord Kelvin, connected all three of the thermoelectric coefficients together in the Kelvin relationships. These equations describe how the Seebeck, Peltier, and the Thomson coefficients are interrelated. These are as follows:

$$S_{ab} = \frac{\pi_{ab}}{T},$$ (relates Seebeck coefficient to Peltier coefficient)

$$\frac{dS_{ab}}{dT} = \frac{\beta_a - \beta_b}{T},$$ (relates Seebeck coefficient with Thomson coefficient)

β $\, ¿\frac{d\pi}{dt}\,$ **− S**,(relates Seebeck coefficient and Peltier coefficient with Thomson coefficient)

The Thomson effect and the Kelvin relationships complete the theory encompassed by the thermoelectric phenomena [29,30,35,36].

Although the Seebeck, Peltier, and Thomson coefficients can describe a material's thermoelectric properties, but they do not contain the information that enables comparison between two different materials. The thermoelectric coefficients do not include thermal and electrical conductance, which are intrinsic characteristics specific to a particular material. Seebeck and Peltier are bulk phenomena, i.e. they depends on bulk rather than surface properties of the materials. Finally, we are interested in calculating the magic number of dimensionless figure-of-merit
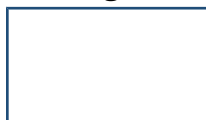
ZT= $\dfrac{S^2 \sigma T}{\lambda}$

where T, σ, S, λ are absolute temperature (T), electrical conductivity (σ), seeback coefficient (S) and thermal conductivity (λ) include mainly two components: an electronic contribution due to the movement of carriers (λ_e), and a lattice contribution via the phonons $\overset{\lambda}{\underset{¿}{¿}}$) i.e ($\lambda = \lambda_e + \lambda_l$), $S^2\sigma$ is

commonly referred to as thermopower. Z has the units of inverse temperature, so it is generally quoted as ZT, with T the absolute temperature. The present challenge is to find material with higher ZT performance, since in most of the materials thermo electric effect is too small to be useful. Moreover any modification to any one of the three (σ, S, λ) parameter would adversely affect the other transport coefficients so that the resulting ZT does not vary significantly.

Chapter 3

Computational Details

3.1 The LAPW method:

For performing electronic structure calculations for crystals, most popular and one of the accurate method's among different methods is the linearized augmented plane wave (LAPW) method. LAPW

was described by Schwarz et al, and it is an improvement over Augmented Plane Wave (APW) developed by Slater. It is based on the density functional theory for the treatment of exchange and correlation and uses e.g. the local spin density approximation (LSDA), which is an efficient and accurate scheme for solving the many-electron problem of a crystal with a fixed nuclei. The LAPW method is a procedure for solving many-electron system by introducing a basis set. It solve the Kohn-Sham equations for the ground state density, total energy, and eigenvalues (energy bands) [37].

Basis set are especially adapted to the problem and this is achieved by dividing the unit cell into two regions

(I)   non-overlapping atomic spheres (centred at the atomic sites) and
(II)   an interstitial region

In the two types of regions different basis sets are used, "Basis" Consists of Plane waves in the Interstitial and Radial Functions in the Spheres.
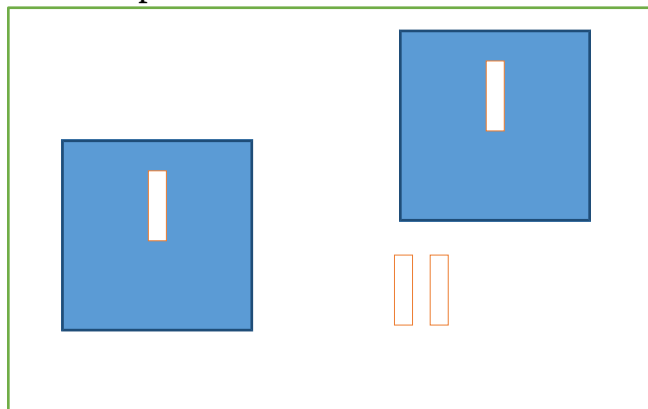

Fig. 3.1: Partitioning of the unit cell into atomic spheres (I) and an interstitial region (II)

(i) Inside atomic sphere t, of radius R_t, a linear combination of radial functions times spherical harmonics Y_{lm} (r) is used

$$k_n = \sum_{lm} \left[\overset{A_{lm} u_{l(r,E_l)}}{\underset{\varphi_{\dot{c}}}{\dot{c}}} + B_{lm} \mathring{u}_{l(r,E_l)} \right] Y_{lm}$$

Where $u_{l(r,E_l)}$ is the radial solution of Schrodinger's equation at the energy of interest (i.e. the band energy) and spherical part of the potential inside the sphere, ů(r) = $\frac{\partial u_l}{\partial E_l}$ is the energy derivative of

u_l taken at the same energy E_l, $\mathring{u}_{l(r,E_l)}$ is introduce for additional freedom, to overcome the problem with the APW method i.e the energy dependence of the secular equation and also to extends variations in the potential. A linear combination of these two functions constitute the linearization of the radial

function, coefficient A_{lm} and B_{lm} are function of k_n determined by matching the value and derivative of the basis functions at the sphere boundary, $u_{l(r,E_l)}$ and $\mathring{u}_{l(r,E_l)}$ are obtained by numerical integration of the radial Schrodinger equation on a radial mesh inside the sphere.

(i) In the interstitial region a plane wave expansions in free space is used

$$\varphi_{k_n} = \frac{1}{\sqrt{\omega}} e^{ik_n t}$$

where k_n = k + K_n , K_n are the reciprocal lattice vectors and k is the wave vector inside the first Brillouin zone. Each plane wave is augmented by an atomic-like function in every atomic sphere.

The solutions to the Kohn-Sham equations are expanded in this combined basis set of LAPW's according to the linear variation method

$$\Psi_k = \sum c_n \Phi_{k_n}$$

and the coefficients c_n are determined by the Rayleigh-Ritz variational principle.

In plane wave the accuracy of the basis set was determine by K_{max} , where as in the linearized augmented plane wave (LAPW) method the convergenceof this basis set is controlled by a cut off parameter $R_{mt} K_{max}$ = 6 - 9, where R_{mt} is the smallest muffin tin sphere radius in the unit cell and K_{max} is the magnitude of the largest K vector.

3.2 Methods of Calculation:

The electronic band structures were calculated by means of the full-potential linear augmented plane wave (FP-LAPW) method based on first-principles density functional theory as implemented in the WIEN2k suite of program [37]. The standard exchange-correlation potential of Local-Density approximation (LDA) and Generalized Gradient Approximation (GGA) schemes for the exchange-correlation underestimate the band gaps of semiconductors, we used modified GGA known as the Tran-Blaha modified Becke-Johnson potential (TB-mBJ)[38-39]. The muffin-tin spheres radii of the structure are taken to be 2.5 $\overset{A}{}$ for A= Sr, 1.6 $\overset{A}{}$ for F, 2.0 $\overset{A}{}$ for M=Ag and 2.2 $\overset{A}{}$ for Ch = S,Se,Te. The plane-wave expansion with radius of muffin-tin sphere (R_{MT}) and(K_{MAX}) i.e $R_{MT} * K_{MAX}$ equal to 7. The crystal structure of SrFAgCh (Ch=S,Se,Te)is tetragonal with space group P4/nmm(No.129). The complete structural optimization has carried out using the experimental parameters [24] to get the theoretical lattice parameters with an energy convergence criterion of 10^{-6} Ry per formula unit. For k-space integrations 12*12*5 k-mesh was used for the Monkhorst-Pack scheme. The self-consistent calculations included spin-orbit coupling. The carrier concentration (p for holes and n for electrons)and temperature (T) dependent thermoelectric properties like thermopower (S), electrical conductivity scaled by relaxation time $\frac{\sigma}{\tau}$ were calculated using BOLTZTRAP [40] code, within Rigid Band Approximation (RBA) [41-42] and the constant scattering time (τ) approximation (CSTA). In RBA the band structure is assumed unaffected by doping, which only leads to a shift of the chemical potential. For semiconductors it is a good approximation for the calculation of the transport properties, when the doping level is not too high [30,43,44]. In the CSTA, the scattering time of electrons is assumed independent of the electron energy, while it may depend on carrier concentration and temperature. A detailed discussion of the CSTA is given in [45-47]. The only situation where the CSTA can fail is when bipolar conduction is significant, which happen in narrow-gap materials.

Chapter 4

Results and Discussions

4.1.Structural Properties:

Initially experimental lattice parameters were used to generate tetragonal crystal structure of SrAgFCh (Ch = S,Se,Te). The crystal structure of SrAgFS is shown in Fig-4.1.
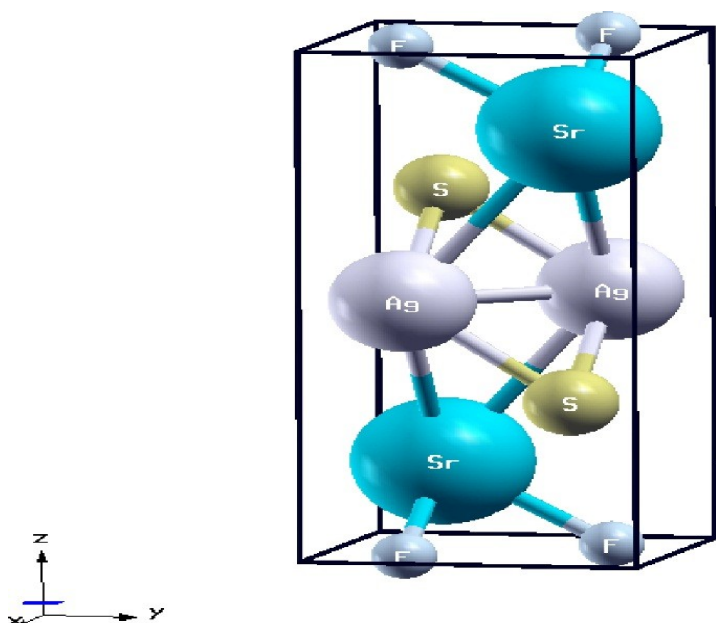

Fig-4.1: The crystal structure of SrAgFS

The complete structural optimisation has been carried out using the experimental parameters [24]. The obtained lattice parametersare in reasonable agreement with the experimental reported values as well as with the other theoretical calculations see Table 1. As mentioned earlier the theoretical GGA-band gaps will underestimate compared to the experiment, our band gap results with GGA are also shown the same, which is consistent with the other calculations. On the other hand, the calculated band gaps with the TB-mBJ potential are in good agreement with the experimental reports. This shows the success of the TB-mBJ potential in predicting the accurate band gaps closed to experiment. We also calculated the bulk modulus (B) for all the compounds and are given in the table. From these we found that the bulk modulus SrAgFS is high compared to the other compounds and it is found to decrease down the group $(B^{S} > B^{Se} > B^{Te})$.

4.2.Band Structure and Density of States

The electronic structure calculations are carried out with the optimised lattice parameters. As mentioned above, the standard methods of the LDA/GGA calculations underestimate the band gaps of the semiconductors or insulators. We have calculated the electronic properties using TB-mBJ functional, which is quite successful in predicting the band gaps of the materials very close to the experiments. The calculated band structures of SrFAgCh along the high symmetry directions of the tetragonal Brillouin zone are shown in Fig.4.2. The over all profile of all the bands remain same in each case. The effect of spin-orbit coupling on the present compounds has shown a significant changes at the Γ point which compare very well with the work of Bannikov et. al[23]. The SOC splitting energy of the degenerate bands is found to be 31meV for S, 129 meV for Se and 330 meV for Te, which is found to be little higher in comparison with the other 1111 family of compounds BaCuChF [49], which may due to the usage of different exchange correlation functional. The SOC energy is found to increase as the mass of the chalcogen increases. As we mentioned earlier that the above mentioned compounds crystallise in the tetragonal structure, Γ-X direction in the Brillouin zone indicate the crystallographic ab- plane and Γ-Z direction indicate the c- axis of the tetragonal crystal structure. Important feature to note is that the valence band maximum (VBM) and conduction band minimum (CBM) are both located at the centre of the Brillouin zone i.e at the Γ-point, thus making these compounds direct-band-gap semiconductor with Γ - Γ inter-band transitions. Band gap $\dfrac{E}{(¿¿g)}{¿}$ values are found to vary non-monotonously from S to

Te, in the group.From the band structure we can also see clearly that the high-symmetry directions of Γ-Z, R-X, M-A shows a complete flat-band, which might indicated a good thermopower. The flat band along Γ-Z near Fermi level will contribute to the thermopower whereas the less dispersive band along Γ-X direction will contribute to the electrical conductivity. We moved to further analysis the character of this flat band region. The top of the valance band is the combination of the both Ag-d and chalcogen-p bands which suggest a strong hybridisation between these two bands which is also confirmed from the density of states as mentioned below. A similar situation is seen for the other two compounds also, they have almost similar band structure. From this we can conclude that the contribution to the flat bands are due to the amalgamation of Ag-d and chalchogen-p bands. The CBM contribution is derived from the Sr-d orbitals and there is no contribution from any of the other elements present in the compounds.

The calculated density of states (DOS) along with the partial density of states of each of the elements for all the three compounds are shown in Fig.4.3. The DOS shows that the maximum contribution to the total DOS is due to the Ag-d and chalcogen-p states at the VBM as seen from band structure for all the three compounds. The extent of the peak at the VBM is found to decrease as we move from S to Te, which may be due to the increase in the splitting energy of SOC from S to Te. The CBM is mainly due to the Sr-d states for all the investigated compounds. The electronic structure properties shows hybridisation of the Ag-Ch combination at the VBM which is a combination of heavy and light bands at the Fermi level and in general one can except good thermoelectric properties from these compounds.

Table 1:Ground state properties of SrAgFCh (Ch=S,Se,Te) with GGA functional along with the available experimental and other calculated results.

SrAgFS	Present	Experiment[a]	Other Calculations[b]
a (Å)	4.2024	4.0593	4.114
c (Å)	8.7528	9.1521	9.148
V (Å^3)	154.576(+2.5%)	150.81	154.830(+2.6%)
z (Sr)	0.15654	0.1534	
z (S)	0.69213	0.6945	
B (GPa)	64.28		
Band gap (eV)	1.185(GGA) 2.53(TB-mBJ)		1.251(GGA)
SrAgFSe	Present	Experiment	Other Calculations
a (Å)	4.3086	4.1652	4.205
c (Å)	8.8956	9.2552	9.367
V (Å^3)	165.138(+2.8%)	160.57	165.627(+3.1%)
z (Sr)	0.15060	0.1500	
z (Se)	0.69755	0.6959	
B (GPa)	59.01		
Band gap (eV)	1.032(GGA) 2.27(TB-mBJ)		1.088(GGA)
SrAgFTe	Present	Experiment	Other Calculations
a (Å)	4.4218	4.3397	4.368
c (Å)	9.4880	9.5947	9.758
V (Å^3)	185.512(+2.7%)	180.70	186.177(+3.0%)
z (Sr)	0.13738	0.1358	
z (Te)	0.69911	0.6976	
B (GPa)	51.87		
Band gap (eV)	1.319(GGA) 2.334(TB-mBJ)		1.333(GGA)

a: Ref. 23; b: Ref. 24;

SrAgFS

(a)

SrAgFSe

SrAgFTe
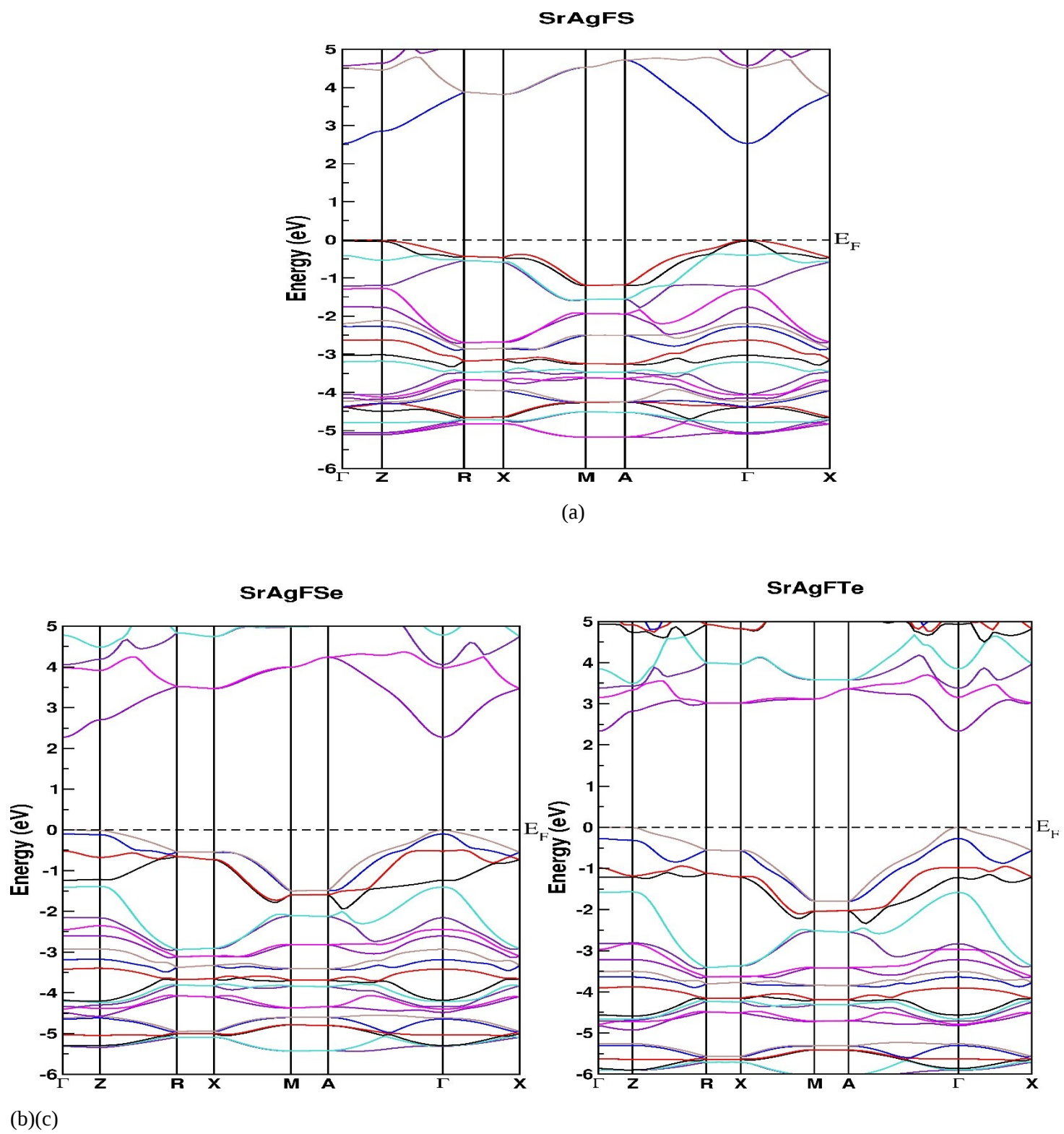

(b)(c)

Fig -4.2: Calculated band structure of SrAgFCh (a) S (b) Se and (c) Te
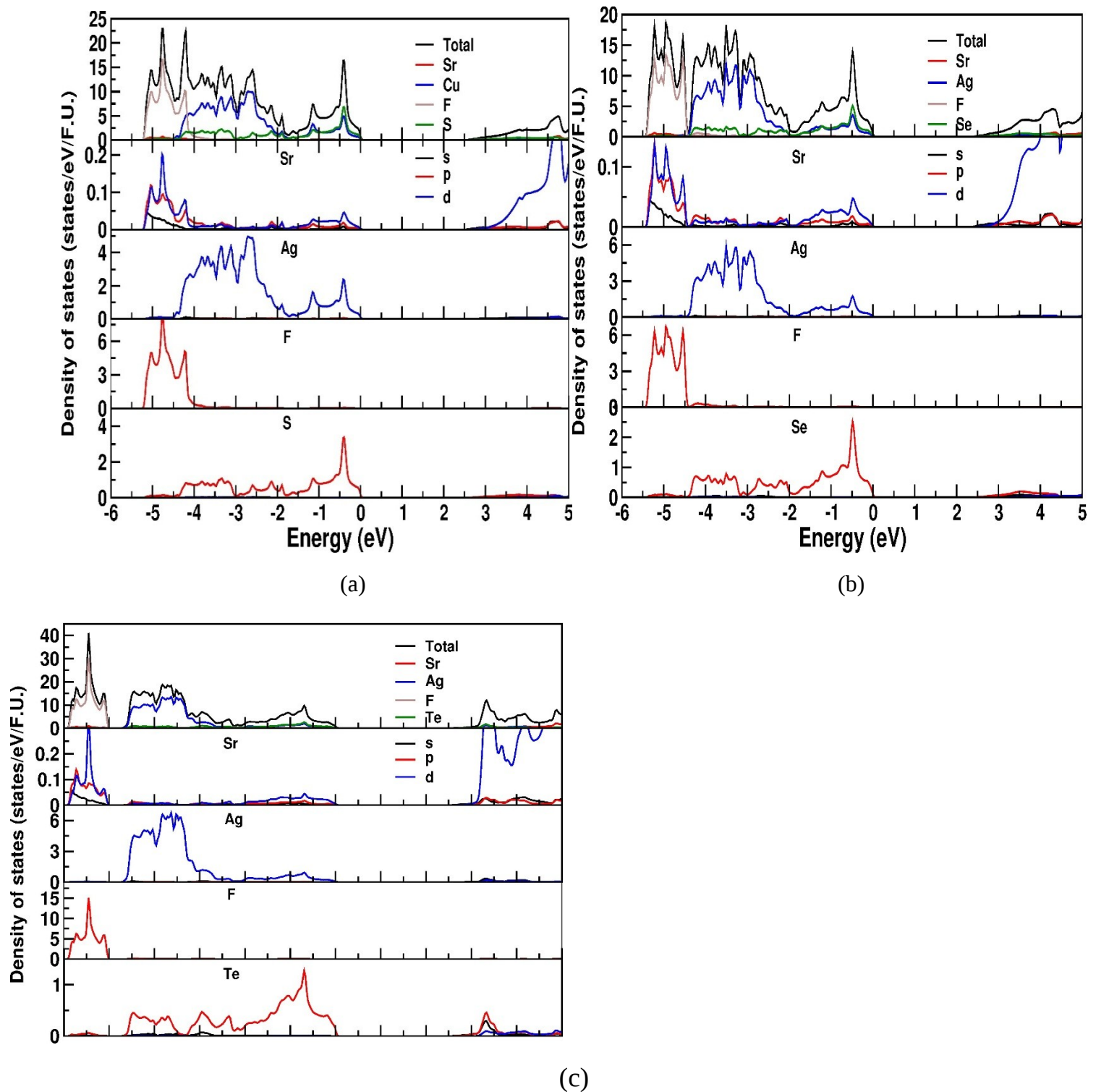
(a)

(b)

(c)

Fig -4.3: Calculated Density of states of SrAgFCh (a) S (b) Se and (c) Te

## 4.3. Thermoelectric properties

4.3.1 Thermopower:

The carrier concentration and temperature dependent thermoelectric properties of SrAgFCh are obtained by solving the Boltzmann transport equation as implemented in the BOLTZTRAP code [40]. All the properties are calculated using Rigid Band Approximation (RBA) [41,42] and the relaxation time τ is assumed to be independent of energy [45-47]. The calculated propertiessuch as thermopower and electrical conductivity scaled by the scattering time (i.e.($\frac{\sigma}{\tau}$)), as functions of carrier concentration both electron and hole, at various temperature along the crystallograpic axis of a(xx) and c(yy)- axes are shown in Fig. 4.4, 4.5. As there are only few studies available on these compounds we could not find the melting point of these compounds. The thermoelectric properties of the prototype compounds of BiCuOCh [48] are well studied upto 1000 K, so we have studied the present compounds upto 900 K. All the properties are given in the optimum working region of the concentration i.e.

1×10^{18} to 1×10^{21} cm⁻³for both electrons and holes. The trend of the thermopower for both electron and hole concentration is similar to what has been found for other thermoelectric materials with tetragonal structure. It is also seen that the thermopower increases with decreasing carrier concentration. The Pisarenko behaviour, i.e. logarithmic variation of the thermopower with carrier concentration, is found in the range of $10^{18} - 10^{21} cm^{-3}$, which is optimumworking region for good thermoelectric materials. From Fig. 4.4, we found that the thermopower value are found to vary from 670-870 $\frac{\mu V}{K}$ for the hole concentration in the temperature range of 300 to 900 K at a hole concentration of 1×10^{18}, whereas for electron it is found to be in the range of 420-670 $\frac{\mu V}{K}$. We find a non-monotonous variation in the low temperature region (at 300 K), so for better applications one could look at the thermopower above 300 K, which shows a regular trend of the thermoelectric behaviour. As we can notice very clearly, that the difference along the a- and c- axis for the hole concentration is very high, which is due to the dispersion of the bands being different in this direction. From the band structure the band along Γ-Z is less dispersive and one could expect a high thermopower in this direction as seen from Fig-4.4(b), whereas a light dispersion along the Γ-X direction will have a low thermopower value compared to the Γ-Z direction. In contrast, the thermopower values of the electron doping is found to be varying in between -420 to-670 $\frac{\mu V}{K}$ in the same range of temperature and for a similar concentration as mentioned above for holes. The electron concentration is found to vary in similar trend as holes and is found to increase as temperature increase, but very low as compared to the hole concentration which is mainly dependent on dispersion of the bands in the conduction band. The anisotropy is found to be lowin the case of electrons doping compared to hole doping. The thermopower is found to decrease as we move from S to Te in the group for both the carrier concentrations. As a whole we find a good thermopower in the hole concentration region for all the compounds.
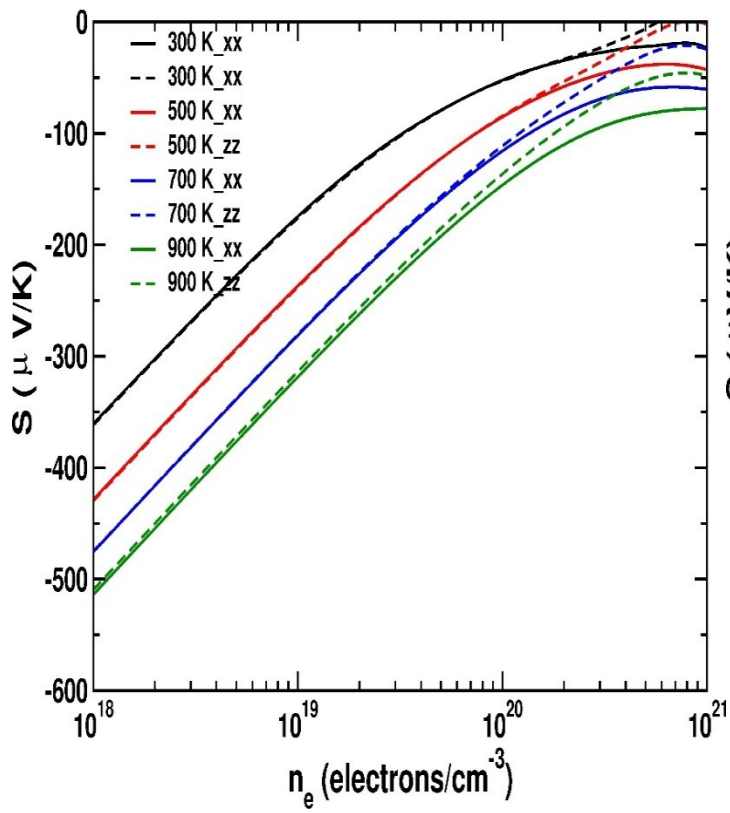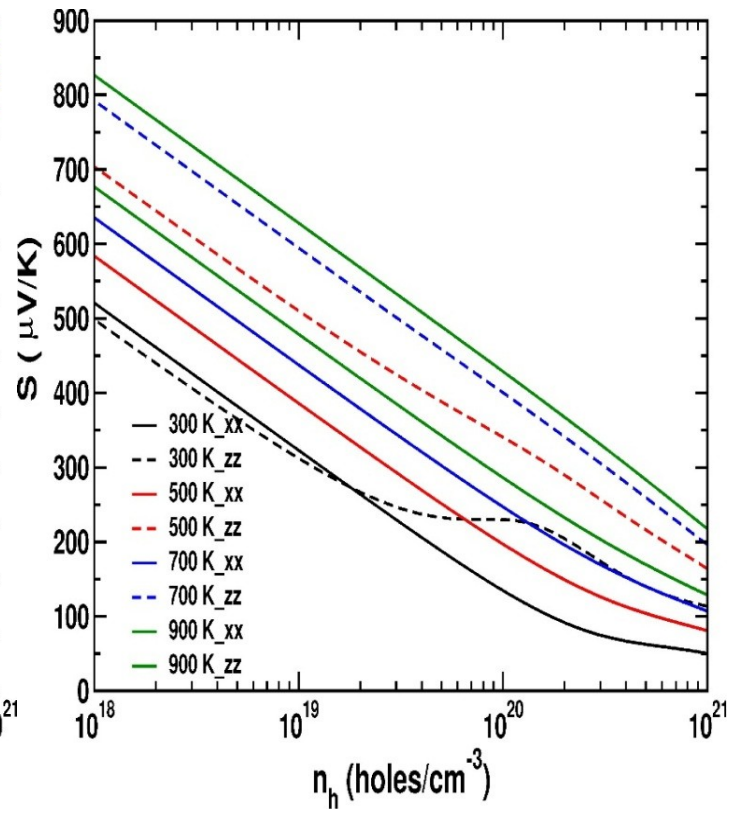

(a)

(b)
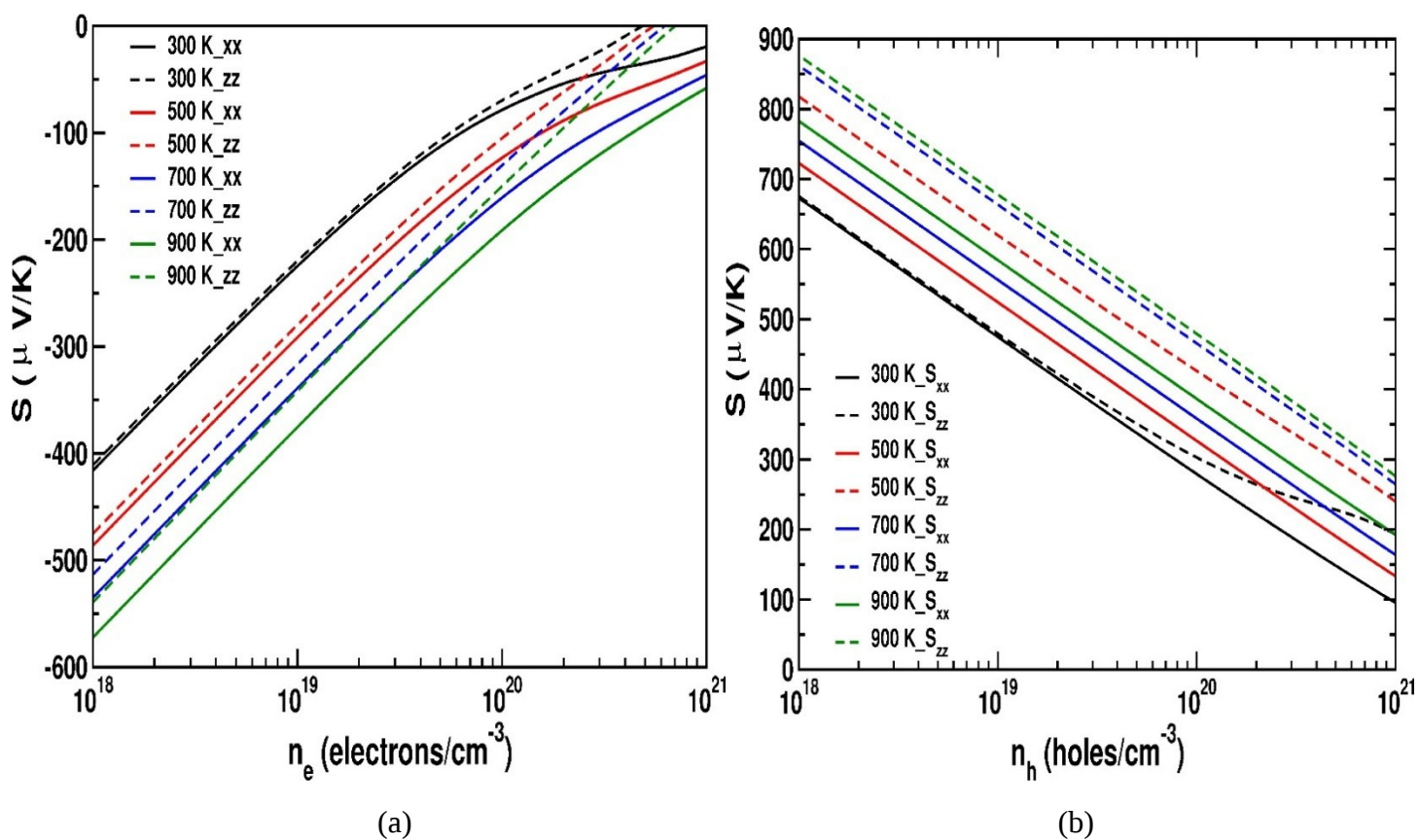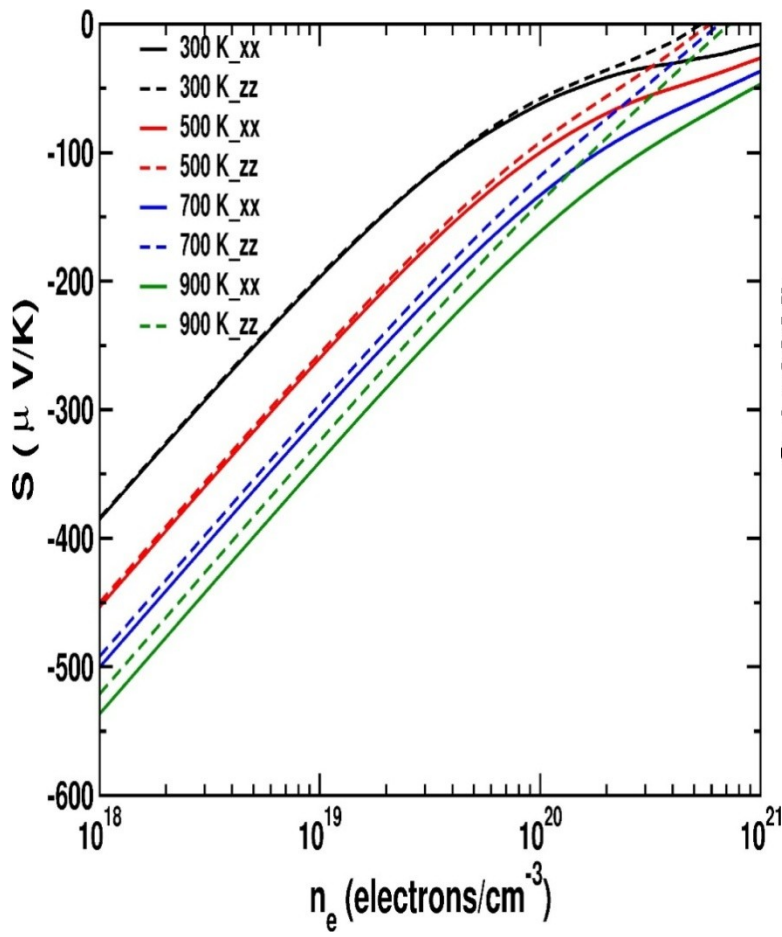
(c)
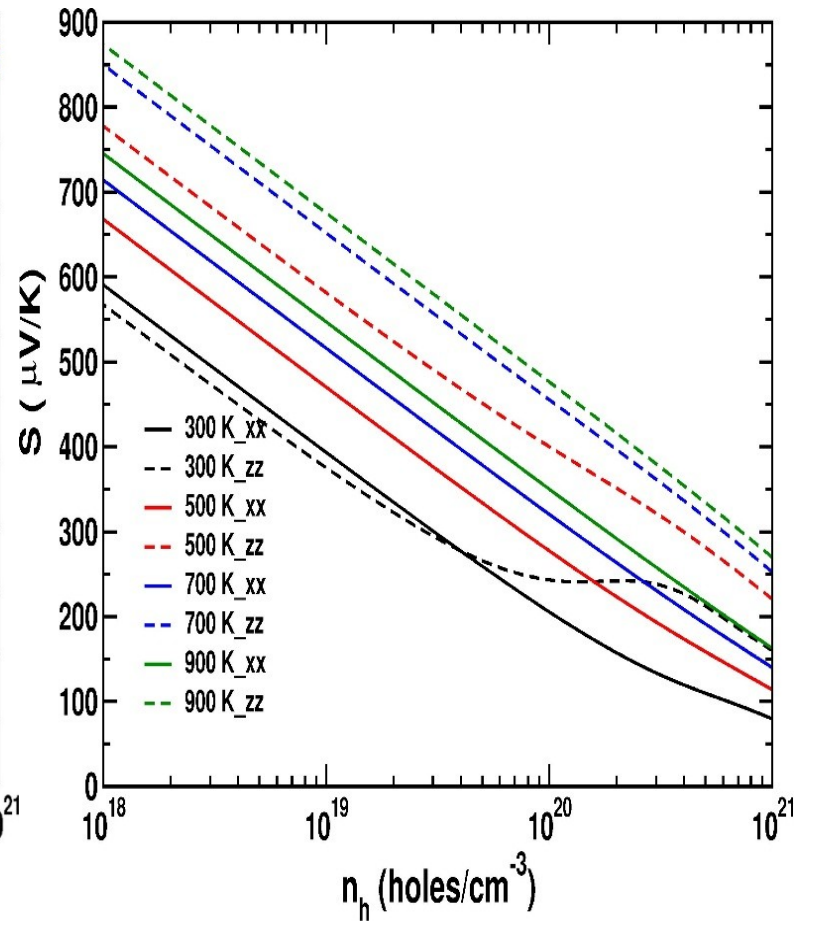
(d)

(e)(f)

Fig.4.4. Thermopower of SrAgFS (a) electrons (b) holes, SrAgFSe (c) electrons and (d) holes and SrAgFTe (e) electrons and (f) holesalong X- and Z-axis
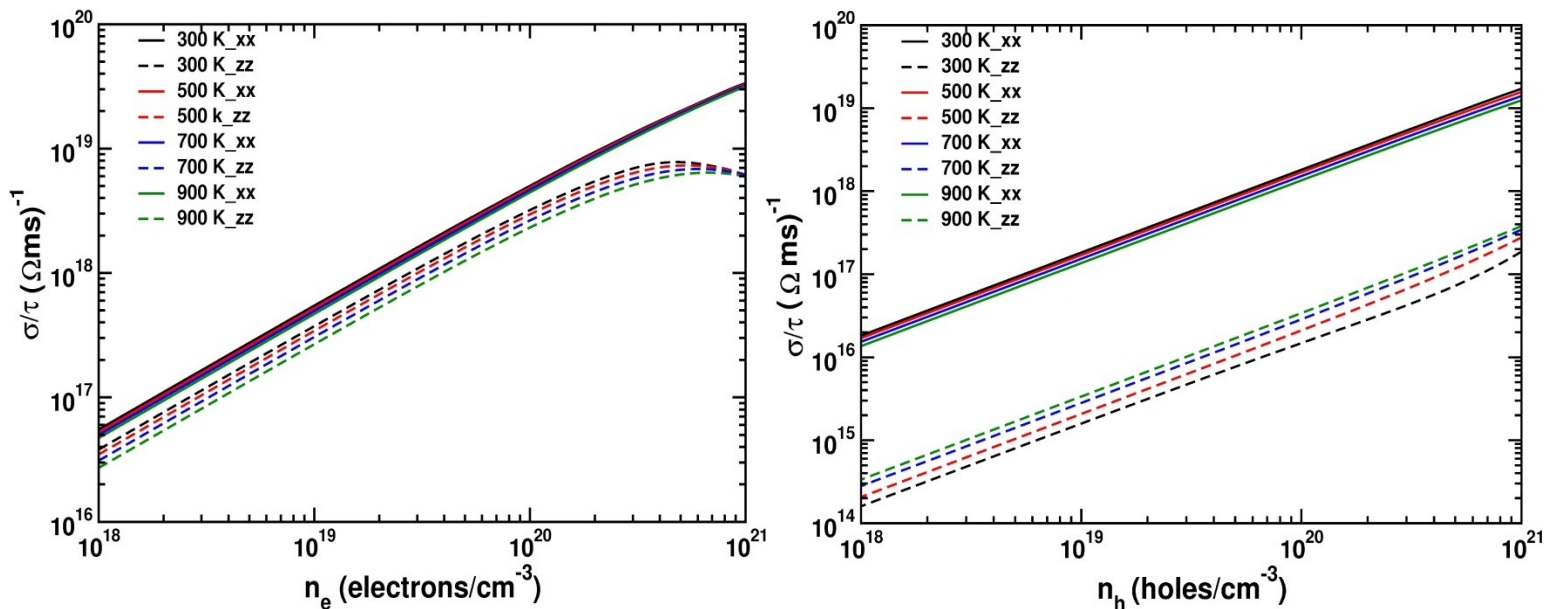
4.3.2 Electrical Conductivity

The electrical conductivity of SrAgFCh is shown in fig 4.5 for both the electron and hole concentration, respectively. Similar scenario is found for both electron and hole doping with in the optimum working range of the concentration and we find a decrease in the electrical conductivity at the high concentration region, so we stick to the lower concentration region ($< 10^{21}$) for better applications. As we expected from the band structure the electrical conductivity in the hole concentration is high along the a-axis compared to the c-axis, because the dispersion along the Γ-X is more compared to the Γ-Z which shows an isotropy along a,b,c axis. As there is no great difference in the conduction band we could expect less anisotropy in the case of electron concentration. We also found the electrical conductivity to be high in case of the electron doping compared to the hole doping approximately of two order's. Similar to sulphur we found the other two chalcogen elements also to behave same which are shown in Fig. 4.5 (c,d,e,f). The electrical conductivity is found to be increase as we move down the group from S to Te, which is regular trend in the periodic table.

The thermopower value is found to be highin the c-axis and the electrical conductivity is low in the same direction, whereas the high electrical conductivity in the a- axis will increasethe power-factor i.e. $\frac{S^2\sigma}{\tau}$ in these direction compared to the a- axis even with low thermopower. We found optimum values for hole concentration of 8.27 $\times$ 10^{20}cm^{-3} with a thermopowervalue of 177µV/K and electrical conductivity of 1.14×10^{19}(Ωms)$^{-1}$. The thermopower and the electrical conductivity are found to be of the same orderas that of Zuo et. al.[48]. As BiCuChO compounds exhibit a low thermal conductivity, we may except that ifthermal conductivity of SrAgChF (as they are similar type of compounds) could also be low thenit would allow us to predict that these materials will also have a goodthermoelectric properties of the same order of BiCuChO for better applications.

(a)   (b)
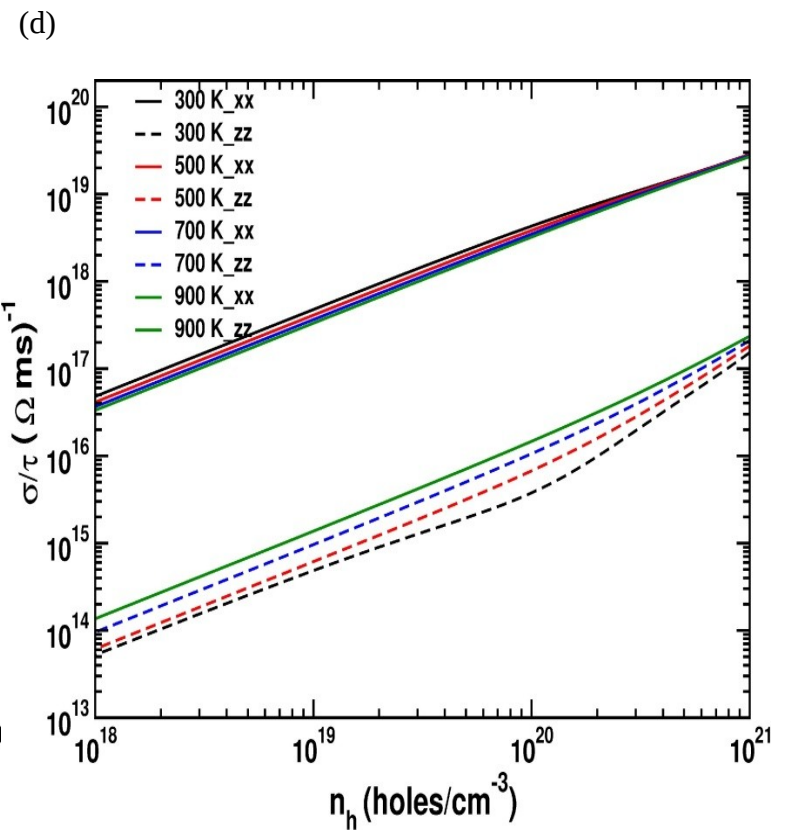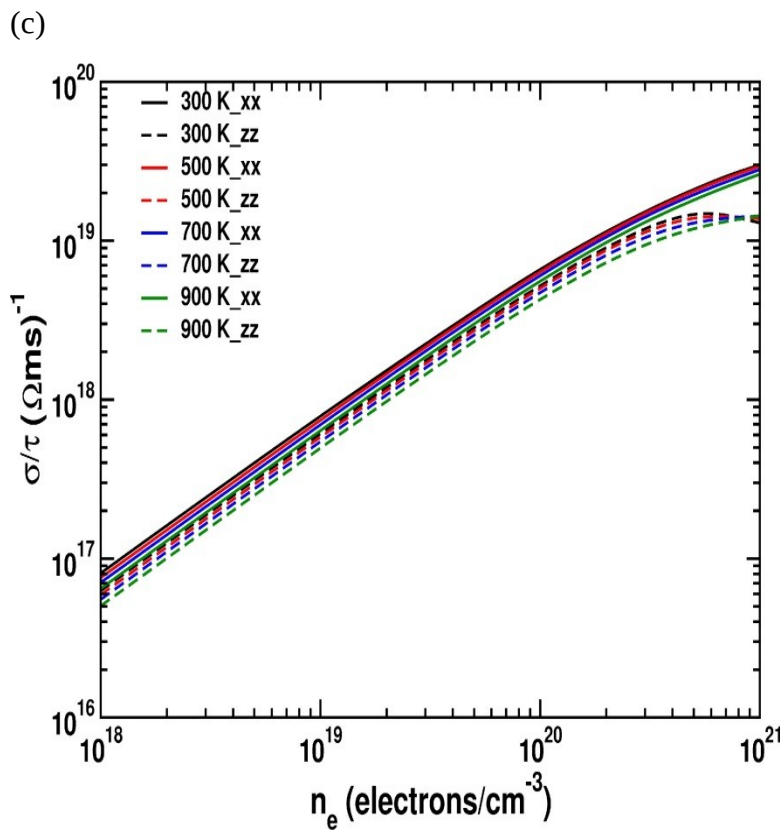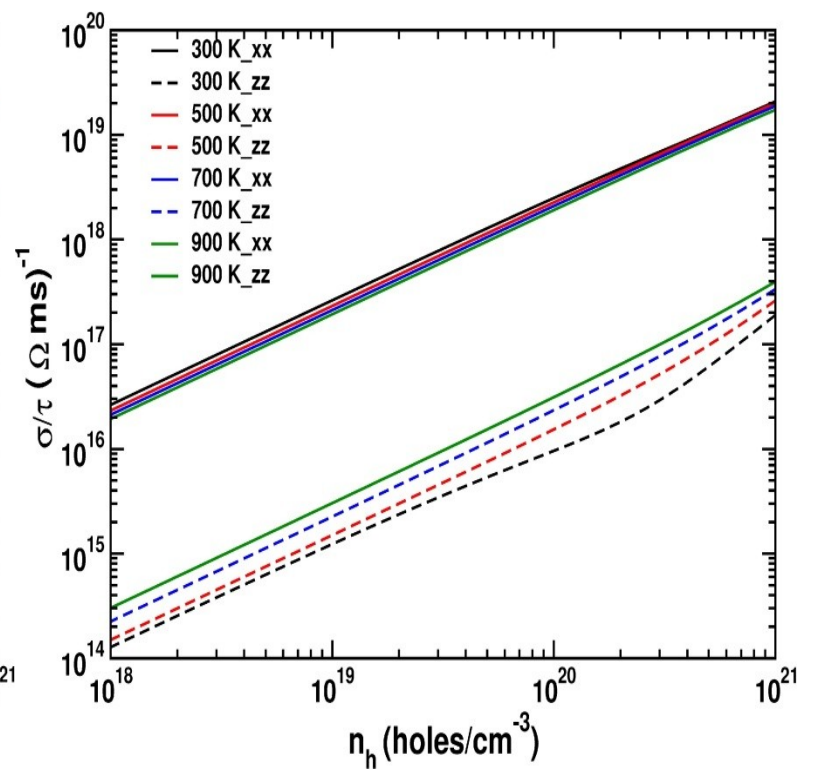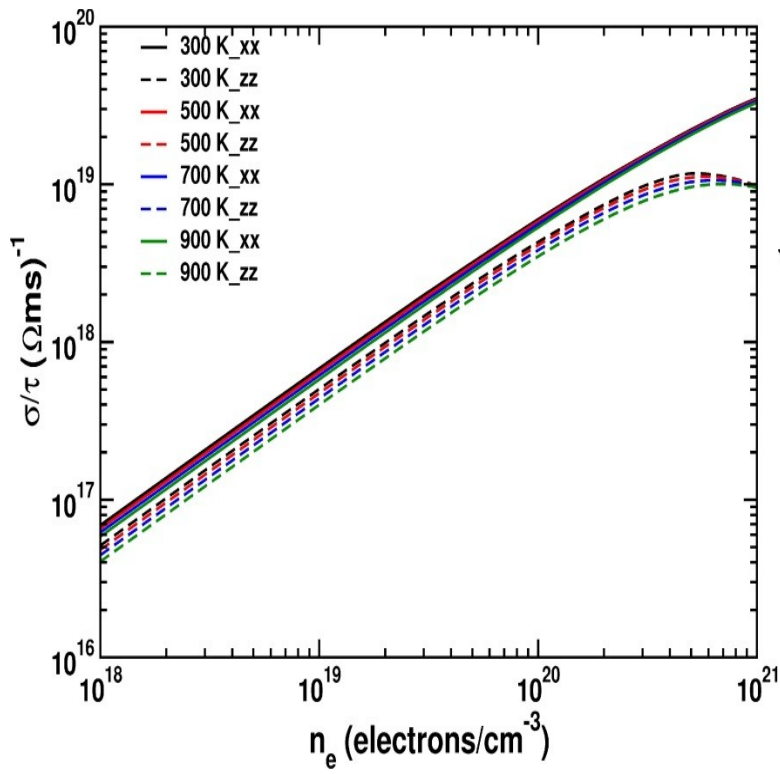
Fig-4.5. The calculated electrical conductivity scaled by relaxation time of SrAgFS (a) electrons (b) holes, SrAgFSe (c) electrons and (d) holes and SrAgFTe (e) electrons and (f) holesalong X- and Z-axis

Chapter 5

Conclusions and Future directions

The electronic transport properties of SrAgChF were calculated using density functional theory. The calculated spin-orbit splitting of degeneracy is found to be quite significant and is well within the order of the other BaCuFChcompounds. All the investigated compounds were found to be direct wide-band gap semiconductors which is in good agreement with the experiment. The top of the valence band is found to be the combination of the both transition metal-d and chalcogen-p bands, which shows the strong hybridisation among these two bands. We have calculated the thermoelectric properties using BoltzTraPcode. The thermopower is found to decrease as we move from S to Te, incontrast to these the electrical conductivity is found to be increase with increasing concentration. The hole concentration shows a high thermopower compared to the electron concentration, which shows that the investigated compounds are found to be more favourable for hole doping.We found a optimum values for a hole concentrations of 8.27×10^{20} cm^{-3} with a thermopower value of 177 µV/K and electrical conductivity of 1.14×10^{19} (Ωms)$^{-1}$which is found to be in good agreement with BiCuOCh.As BiCuChO compounds exhibit a low thermal conductivity, we may except that ifthermal conductivity of SrAgChF (as they are similar type of compounds) is also low then we may predict that these materials will also have a goodthermoelectric properties of the same order of BiCuChO for better applications. Doping other atom on site Sr might enhance the thermoelectric propeties of the present investigated compounds, which may show better thermoelectric applications which might be taken as future work.

Bibliography

1. A. Majumdar, Science 303, 777-778 (2004)

2. L. E. Bell, Science 321, 1457-1461 (2008)

3. G. J. Snyder, and E. S. Toberer, Nat. Mater. 7, 105-144 (2008)

4. M. Zebarjadi, K. Esfarjani, M. S. Dresselhaus, Z. F. Ren, and G. Chen, Energy Environ. Sci. 5, 5147-5162 (2012)

5. V. Johnson, W. Jeitschko, J. Solid State Chem. 11, 161–166 (1974)

6. A. T. Nientiedt, W. Jeitschko, Inorg. Chem. 37, 386–389 (1998)

7. K. Kayanuma, R. Kawamura, H. Hiramatsu, H. Yanagi, M. Hirano, T. Kamiya, H. Hosono, Thin Solid Films 516, 5800–5804 (2008)

8. D. Johrendt, R. Pöttgen, Angew. Chem. Int. Ed. 47, 4782–4784 (2008)

9. R. Pöttgen, D. Johrendt, Z. Naturforsch. B. 63, 1135–1148 (2008)

10. J. F. Wager, D. A. Keszler, and R. E. Presley, Transparent Electronics Springer, Berlin (2008)

11. Y. Kamihara, T. Watanabe, M. Hirano and H. Hosono, J. Am. Chem. Soc. 130, 3296 (2008)

12. M. Yasukawa, K. Ueda and H. Hosono, J. Appl. Phys. 95, 3594 (2004)

13. H. Hiramatsu, K. Ueda, H. Ohta, T. Kamiya, and M. Hirano, Appl. Phys. Lett. 87, 21110 (2005)

14. J. A. Spies, R. Schafer, J. F. Wager, P. Hersh, H. A. S. Platt, D. A. Keszler, G. Schneider, R. Kykyneshi, J. Tate, X. Liu, A. D. Compaan, and W. N. Shafarman, Sol. Energy Mater. Sol. Cells. 93, 1296 (2009)

15. Rainer Pottgen, Drik Johrendt, Z. Naturforsch, 63B, 1135-1148 (2008)

16. Wang, C. et al., Europhys. Lett. 83, 67006 (2008)

17. Ren, Z.-A. et al. Chin. Phys. Lett. 25, 22152216 (2008)

18. Yanagi, H. et al. Phys. Rev. B 77, 224431 (2008)

19. Xu, G., Ming, W., Yao, Y., Dai, X., Zhang, S.-C. and Fang, Z., Europhys. Lett. 82, 67002 (2008)

20. Kabbour, H., Cario, L., Jobic, S. and Corraze, B. J. Mater. Chem. 16, 4165-4169, (2006)

21. Motomitsu, E., Yanagi, H., Kamiya, T., Hirano, M. and Hosono, H. J. Solid State Chem. 179, 1668-1673, (2006)

22. Park, C.-H., Kykyneshi, R., Yokochi, A., Tate, J. and Keszler, D. A. J. Solid State Chem. 180, 1672-1677, (2007)

23. Bannikov, V.V., Shein, I. R., Ivanovskii, A. L., J. Solid State Chem. 196, 601-606, (2012)

24. D. O. Charkin, A. V. Urmanov, S. M. Kazakov, J. Alloys Compound. 516, 134 (2014)

25. Hohenberg P. and Kohn W., Phys. Rev. B 136, 864-871, (1964)

26. Kohn W. and Sham L. J., Phys. Rev. A 140, 1133-1138, (1965)

27. Lundqvist S. and Marc N. H., ' Theory of the Inhomogeneous Electron Gas', Plenum, (1983)

28. C. Godart, A. P. Gonçalves, E. B. Lopes, B. 'Villeroy , Role of structures on thermal conductivity in thermoelectric material' , (2008)

29. M. S. Dresselhaus, Solid State Physics Part I, Transport Properties of Solids, (2001)

30. Ziman, Principles of the Theory of Solids, Cambridge Publication, (1972)

31. Reif, Fundamentals of Statistical and Thermal Physics, McGraw-Hill, pp. 393-397, (1965)

32. D. M. Rowe, in Thermoelecrics handbook: macro to nano, edited by D. M. Rowe (Taylor and Francis, Boca Raton), pp. 1-1 thru 1-9, (2006)

33. D. Emin, in Thermoelectrics handbook: macro to nano, edited by D. M. Rowe (Taylor and Francis, Boca Raton), pp. 5-2, (2006)

34. L. D. Hicks and M. S. Dresselhaus, Phys. Rev. B. 47, 12727 (1997)

35.N. W. Ashcroft and N. D. Mermin, Solid State Physics, Cambridge Publication, (1995)

36. "First principles study of thermoelectric properties of zinc-oxide nanowires" Presented to the Graduate Council of Texas State University-San Marcos, (2010)

37. Peter Blaha, Karlheinz Schwarz, Georg Madsen, Dieter Kvasnicka, Joachim Luitz, User's Guide, WIEN2k

38. A. D. Becke, and E. R. Johnson, J. Chem. Phys. 124, 221101 (2006)

39. F. Tran, and P. Blaha, Phys. Rev. Lett. 102, 226401, (2009)

40. G. K. H. Madsen, and D. J. singh, Comput. Phys. Commun. 175, 67-71, (2006)

41. T. J. Scheidemantel, C. Ambrosch-Draxl, T. thonhauser, J. V. Badding, and J.O. Sofo, Phys. Rev. B 68, 125210, (2003)

42. L. Jodin, J. Tobola, P. Pecheur, H. Scherrer, and S. Kaprzyk, Phys. Rev. B 70, 184207, (2007)

43. B. R. Nag, Electron Transport in Compound Semiconductors,Springer-Verlag, Berlin, (1980)

44. D. J. Singh, and I. I. Mazin, Phys. Rev. B 56, R1650 (1997)

45. D. J. Singh, Funct. Mat. Lett. 3, 223-226, (2010)

46. D. Parker, and D. J. Singh, Phys. Rev. B 85, 125-209, (2012)

47. K. P. Ong, D. J. Singh and P. Wu, Phys. Rev. 83, 115110, (2011)

48. Daifeng Zou, Shuhong Xie, Yunya Liu, Jianguo Lin and Jiangyu Li, J.Mater. Chem. A, 1, 8888-8896 (2013)

49. A. Zakutayev, R. Kykyneshi, G. Schneider, D. H. McIntyre, and J. Tate, Phys. Rev. B 81, 155-103, (2010)